Journal of the Chinese Institute of Engineers, Vol. 23, No. 3, pp. 357-368 (2000)

ELASTODYNAMIC BEM MODELLING OF MULTIPLE SCATTERING OF ELASTIC WAVES BY SPATIAL DISTRIBUTIONS OF INCLUSIONS

Enru Liu[1*] and Zhongjie Zhang[2]

[1*]*British Geological Survey, Murchison House, West Mains Road Edinburgh EH9 3LA, Scotland UK*

[2]*Institute of Geophysics, Chinese Academy of Sciences 11 Datun Road, Beijing, China 100101*

Key Words: elastodynamic BEM, inclusions, elastic waves, multiple scattering.

ABSTRACT

We use a 2D elastodynamic boundary integral equation or boundary element method (BEM) in this paper and apply it to solve crack scattering problems. The method is based on the integral representation of a scattered wavefield by assuming a fictitious source distribution on the scattering objects or inclusions (i.e. mathematical description of Huygens' principle), and the fictitious source distribution can be found by matching appropriate boundary conditions at the boundary of the inclusions. We present two numerical examples to demonstrate the versatility of the BEM method. The first example shows that different spatial arrangements of the same scatters lead to profound differences in scattering characteristics, in particular the frequency contents of the transmitted wavefields using the method of time-frequency analysis. The second example shows the effects of power-law or fractal distribution of scalelengths on transmitted wavefields, and we conclude that frequency characteristics, such as the frequency of the peak attenuation, can be related to spatial size parameters of the model.

I. INTRODUCTION

When an elastic wave meets an obstacle, it is scattered. If there are several obstacles the wavefield scattered from one obstacle will induce further scattered fields from all the other obstacles, which will induce further scattered fields, from all the other obstacles, and so on. This process is called multiple scattering. The simplest approximation, called single scattering or the Born approximation, is to ignore the multiple scattering field completely. This approximation has been used widely (Hudson, 1977; Hudson and Heritage, 1981). It is only valid for weak scattering or when the obstacles are small compared to both the wavelength and the spacing between the obstacles. Clearly, it has serious limitations when dealing with large scale inclusions or fractures such as in hydrocarbon reservoirs. Several theories exist for the computation of elastic wavefields which take into consideration of multiple scattering, but few are valid for large sizes and short wavelengths except numerical approaches. When the size of inclusions is

*Correspondence addressee

substantially less than wavelengths, various equivalent medium theories are available which produce azimuthal variation of elastic properties if there is a strong alignment of the inclusions (for examples, Hudson 1981). The presence of spatial correlations of different systems cannot be accounted for with any effective medium theory. The use of numerical methods seems to be the only way which is capable of providing accurate solutions without restriction of size to wavelength ratio.

Finite difference methods (FDs) have been used widely in the study of scattering of seismic waves by crustal heterogeneities with continuous variation of physical properties, and they have also been used to model scattering by thin cracks (Fehler and Aki, 1978). However, it is not easy to handle discrete inhomogeneous bodies with FDs. In this paper, we use a method known as the elastodynamic boundary element method (BEM) and show how it can be utilised to compute wavefields from discrete inclusions with various spatial distributions. Note that previous applications of this method to elastodynamics include study of the effects of topography on seismic waves (Sánchez-Sesma and Campillo, 1991; 1993; Yokoi, 1996), wave propagation in laterally and smoothly varying media (Bouchon and Coutant, 1994), scattering of elastic waves by cracks (Bouchon, 1987; Chen and Zhou, 1994; Murai, Kawahara and Yamashita, 1995; and Coutant, 1989); diffraction by hydraulic fractures (Liu, Crampin and Hudson, 1997; Pointer, Liu and Hudson, 1998); and downhole source radiation (Dong, Bouchon and Toksöz, 1995; Dong and Toksöz, 1995).

II. INTEGRAL REPRESENTATION OF ELASTIC WAVEFIELDS

In scattering problems the total wavefield is usually written as the superposition of the scattered field $\boldsymbol{u}^s$ and the free field $\boldsymbol{u}^0$ (i.e. the field in the absence of inclusions):

$$\boldsymbol{u}=\boldsymbol{u}^0+\boldsymbol{u}^s. \tag{1}$$

Considering the domain S surrounding an inclusion, and its boundary L (Fig. 1), the wavefield generated when a steady-state time-harmonic wave is scattered by a void of arbitrary shape in an elastic solid, can be derived using the reciprocal theorem (Cruse, 1968). In the indirect BEM representation, the scattered wavefield can be written as (Coutant, 1989; Sánchez-Sesma and Campillo, 1991; Pointer, Liu and Hudson, 1998):

$$u_i^s(\boldsymbol{x})=\int_L \phi_j(\boldsymbol{x}')G_{ij}(\boldsymbol{x},\boldsymbol{x}')dL',\ i=1,\ 2,\ 3 \tag{2}$$

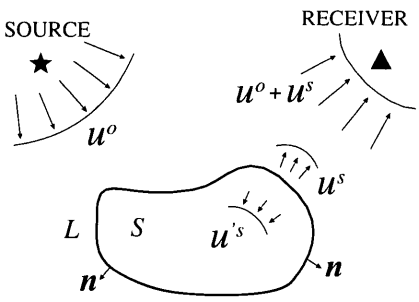

Fig. 1 Problem configuration: A scattering object S bounded by the curve L with outwards normal $\boldsymbol{n}$. Upon an incidence of $\boldsymbol{u}^0$ located at source the total wavefield received at receiver is the superposition of the incident wavefield $\boldsymbol{u}^0$ and the scattered wavefield $\boldsymbol{u}^s$

where u_i^s is the ith displacement of scattered waves at $\boldsymbol{x}$; and ϕ is the fictitious source evaluated at $\boldsymbol{x}'$ on L with outwards normal $\boldsymbol{n}$. Einstein summation convention is understood throughout. $G_{ij}(\boldsymbol{x}, \boldsymbol{x}')$ is the Green's tensor, i.e. the displacement in the ith direction at point $\boldsymbol{x}$ due to the application of a unit force in the jth direction at point $\boldsymbol{x}'$, and is given by (Pao and Varatharajulu, 1976):

$$G(\boldsymbol{x},\boldsymbol{x}')=\frac{1}{4\pi\rho\omega^2}\{k_s^2\boldsymbol{I}g_s(\boldsymbol{x},\boldsymbol{x}')+\nabla\nabla[g_p(\boldsymbol{x},\boldsymbol{x}')-g_s(\boldsymbol{x},\boldsymbol{x}')]\}, \tag{3}$$

where $\boldsymbol{I}$ is unit matrix, and for the 2D wave propagation we have:

$$g_{p,s}(\boldsymbol{x},\boldsymbol{x}')=i\pi H_0^{(1)}(k_{p,s}\,r), \tag{4}$$

where ρ is density, ω is circular frequency, $k_p=w/v_p$, and $k_s=\omega/v_s$ are P- and S-wavenumber, respectively (v_p and v_s are P- and S-wave velocities in solid); $r=|\boldsymbol{x}-\boldsymbol{x}'|$; and $H_0^{(1)}$ is the Hankel function of the first kind of order zero. Explicit Green's tensors can be found in Sánchez-Sesma and Campillo (1991); Pointer, Liu and Hudson (1998).

The traction representation (Banerjee and Butterfield, 1981) is given by:

$$t_i(\boldsymbol{x})=c_t\phi_i(\boldsymbol{x})+\int_L \phi_j(\boldsymbol{x}')T_{ij}(\boldsymbol{x},\boldsymbol{x}')dL',\quad i=1,\ 2,\ 3 \tag{5}$$

where T_{ij} is Green's traction tensor, that is, the traction in the ith direction at point $\boldsymbol{x}$ on the boundary due to the application of a unit force in the jth direction at point $\boldsymbol{x}'$, and is related to the Green's stress tensor by Hooke's law. The coefficient $c_t=0$ when $\boldsymbol{x}$ is not on the boundary L; $c_t=0.5$ when $\boldsymbol{x}$ approaches the boundary L from inside S; and $c_t=-0.5$ when $\boldsymbol{x}$ tends to L from outside, provided the following two

conditions are not violated (Banerjee and Butterfield, 1981; Pointer, Liu and Hudson, 1998): (1) The point $\boldsymbol{x}'$ is not located at any edge or a corner (i.e. there must be a unique tangent plane at $\boldsymbol{x}'$); and (2) The surface integral in Eq. (5) must be understood as a Cauchy principal-value integral.

The above equations deal with the presence of a single inclusions. However, the expression derived for the outward scattered field is still valid for a boundary L made up of N distinct boundaries L^1, L^2, ..., L^n surrounding separate inclusions with surfaces S^1, S^2, ..., S^n. The scattered field expressed by Eq. (2) takes into account the interactions between inclusions, and we obtain the complete multi-scattered wavefield:

$$u_i(\boldsymbol{x}) = \sum_{n=1}^{N} \int_{L^n} \phi_j^n(\boldsymbol{x}') G_{ij}^n(\boldsymbol{x}, \boldsymbol{x}') dL'^n . \tag{6}$$

To achieve the single scattering approximation, we consider that each inclusion is only submitted to the incident wavefield but not to the scattered field radiated by other inclusions. Consequently, when computing the boundary conditions at a discretized point of a given surface, we must cancel in Eq. (6) each term describing the interaction between different inclusions; i.e. by setting the corresponding terms to zero before the inversion of the system.

To evaluate the wavefield inside the inclusions, we treat the interior of each inclusion as an independent medium with no interaction between other inclusions. Eqs. (2) and (5) are the two boundary integral equations governing the solution of any well-posed problem, and the boundary element method based on discretizing Eqs. (2) and (5) is called the indirect BEM because the fictitious source distribution ϕ on L has no physical meaning.

III. DISCRETIZATION AND BEM IMPLEMENTATION

Eqs. (2) and (5) form the basis for the boundary element computation, but they are not useful unless coefficients ϕ on the boundary L are known. To obtain ϕ, we also need to obtain an integral representation similar to Eqs. (2) and (5) for the interior material with an appropriate Green's function (as in general, neither the displacement nor the stress vanishes on the diffracting boundary). The essence of the BEM implementation is to discretize each boundary into a finite number of boundary elements, and the boundary conditions, i.e. the continuity of displacement and stress across all elements, are then applied at each element. In the 2D isotropic case, SH-waves are decoupled from P-SV waves, so we shall treat them separately.

SH-wave case

In a simple antiplane case (SH-waves), the Eqs. (2) and (5) for (i=2) become:

$$u_2^s(\boldsymbol{x}) = \int_L \phi_2(\boldsymbol{x}') G_{22}(\boldsymbol{x}, \boldsymbol{x}') dL' , \tag{7}$$

and

$$t_2(\boldsymbol{x}) = \pm \frac{1}{2}\phi_2(\boldsymbol{x}) + \int_L \phi_2(\boldsymbol{x}') T_{22}(\boldsymbol{x}, \boldsymbol{x}') dL' , \tag{8}$$

and the choice of the sign in the first term of the right side of Eq. (8) depends on whether $\boldsymbol{x}$ is evaluated from inside or outside L. The boundary conditions are the continuity of displacement u_2 and traction t_2 at each element on the boundary L for the solid/solid contact (assuming that the source is located outside the inclusions):

$$u_2^0(\boldsymbol{x}) + u_2^s(\boldsymbol{x}) = u_2'^s(\boldsymbol{x}) \text{ and } t_2^0(\boldsymbol{x}) + t_2^s(\boldsymbol{x}) = t_2'^s(\boldsymbol{x}),$$

$$\text{for } \boldsymbol{x} \text{ on } L, \tag{9}$$

where the terms with prime (′) refer to the material of the interior. Displacements and stresses are calculated from the contribution of fictitious sources for all elements. These boundary conditions are satisfied at the centre of each element in the local co-ordinate system, which is defined such that the normal of each element is the positive axis and a clockwise right-hand co-ordinate system is assumed. In order to calculate the displacement at the nth element due to the source at the mth element, we discretize Eqs. (7) and (8) into M line segments ΔL_m with normal $\boldsymbol{n}_m$ (m=1, 2, ... M) using the Green's function for both interior and exterior materials, and assume the force density per line unit is constant on each segment. We then have:

$$u_2^0(\boldsymbol{x}_n) + \sum_{m=1}^{M} \phi_2(\boldsymbol{x}_m) \int_{\Delta L_m} G'_{22}(\boldsymbol{x}_n, \boldsymbol{x}_m) dL'$$

$$= \sum_{m=1}^{M} \phi_2'(\boldsymbol{x}_m) \int_{\Delta L_m} G'_{22}(\boldsymbol{x}_n, \boldsymbol{x}_m) dL' , \tag{10}$$

and

$$t_2^0(\boldsymbol{x}_n) - \frac{1}{2}\phi_2(\boldsymbol{x}_n) + \sum_{m=1}^{M} \phi_2(\boldsymbol{x}_m) \int_{\Delta L_m} T_{22}(\boldsymbol{x}_n, \boldsymbol{x}_m) dL'$$

$$= \frac{1}{2}\phi_2'(\boldsymbol{x}_n) + \sum_{m=1}^{M} \phi_2'(\boldsymbol{x}_m) \int_{\Delta L_m} T'_{22}(\boldsymbol{x}_n, \boldsymbol{x}_m) dL' . \tag{11}$$

The prime in the second variable in the Green's functions is dropped without causing any confusion.

By manipulating the above two equations, we have:

$$\sum_{m=1}^{M} \phi_2(\boldsymbol{x}_m)\overline{G}_{22}(\boldsymbol{x}_n, \boldsymbol{x}_m) - \sum_{m=1}^{M} \phi_2'(\boldsymbol{x}_m)[\overline{G}'_{22}(\boldsymbol{x}_n, \boldsymbol{x}_m)]$$

$$= -u_2^0(\boldsymbol{x}_n), \tag{12}$$

and

$$\sum_{m=1}^{M} \phi_2(\boldsymbol{x}_m)[\frac{1}{2}\delta_{nm} + \overline{T}_{22}(\boldsymbol{x}_n, \boldsymbol{x}_m)]$$

$$- \sum_{m=1}^{M} \phi_2'(\boldsymbol{x}_m)[\frac{1}{2}\delta_{nm} + \overline{T}'_{22}(\boldsymbol{x}_n, \boldsymbol{x}_m)] = -t_2^0(\boldsymbol{x}_n). \tag{13}$$

The two integrals (12) and (13) contain, respectively, weakly- and strongly-singular kernels associated with displacement and traction Green's tensors, and can be evaluated using the method given by Sánchez-Sesma and Campillo (1991) or Pointer, Liu and Hudson (1998). $\overline{G}_{22}$, $\overline{G}_{22}$, $\overline{T}_{22}$, and $\overline{T}_{22}$ are given in Appendix A. The above two equations can be re-written in the following condensed forms:

$$\sum_{m=1}^{M} \phi_m A_{nm} + \sum_{m=1}^{M} \phi_m' A'_{nm} = u_n^0, \tag{14}$$

and

$$\sum_{m=1}^{M} \phi_m B_{nm} + \sum_{m=1}^{M} \phi_m' B'_{nm} = t_n^0, \tag{15}$$

where we have written:

$$\phi_m = \phi_2(\boldsymbol{x}_m), \text{ and } \phi_m' = \phi_2'(\boldsymbol{x}_m), \tag{16}$$

$$u_n^0 = -u_2^0(\boldsymbol{x}_n), \text{ and } t_n^0 = -t_2^0(\boldsymbol{x}_n). \tag{17}$$

The coefficients A's, B's, A''s and B''s in Eqs. (14-15) are coefficient matrices and are given in Appendix A. The terms on the right side of Eqs. (14-15) given in Eqs. (16-17) are displacements and stress of the incident waves at the surface L.

P-SV wave case

Similarly, in the case of P-SV waves, we have the following boundary conditions for the continuity of normal and shear displacements:

$$u_i^0(\boldsymbol{x}) + u_i^s(\boldsymbol{x}) = u_i'^s(\boldsymbol{x}), \ i=1, 3, \text{ for } \boldsymbol{x} \text{ on } L, \tag{18}$$

and for the continuity of normal and shear stresses:

$$t_i^0(\boldsymbol{x}) + t_i^s(\boldsymbol{x}) = t_i'^s(\boldsymbol{x}), \ i=1, 3, \text{ for } \boldsymbol{x} \text{ on } L, \tag{19}$$

Putting Eqs. (2) and (5) into Eqs. (18-19) and following the same procedure as outlined for the case of the SH-wave incidence above, we can derive a system of linear equations similar to Eqs. (12-13) using the Green's functions for both interior and exterior materials. The detailed derivation is omitted here, and only the final result is given in a condensed matrix form:

$$\sum_{m=1}^{M} \phi_{jm} A_{nm}^{ij} + \sum_{m=1}^{M} \phi_{jm}' A'^{ij}_{nm} = u_{in}^0, \ i=1, 3 \tag{20}$$

and

$$\sum_{m=1}^{M} \phi_{jm} B_{nm}^{ij} + \sum_{m=1}^{M} \phi_{jm}' B'^{ij}_{nm} = t_{jn}^0, \ i=1, 3 \tag{21}$$

where again we have written:

$$\phi_{im} = \phi_i(\boldsymbol{x}_m), \text{ and } \phi_{im}' = \phi_i'(\boldsymbol{x}_m), \ i=1, 3 \tag{22}$$

$$u_{in}^0 = -u_i^0(\boldsymbol{x}_n), \text{ and } t_{in}^0 = -t_i^0(\boldsymbol{x}_n). \ i=1, 3 \tag{23}$$

Coefficient sub-matrices A's, B's, and A''s, B''s in Eqs. (20-21) are given in Appendix B. ϕ_i and ϕ_i' (i=1, 3) are the unknown fictitious surface stress distributions. The terms on the right side of Eqs. (20-21) given in Eqs. (22-23) are the displacements and stress of incident waves on the boundary L.

After solving these linear equations for ϕ on the boundary L, the final step is to compute displacements at any location $\boldsymbol{x}$ outside L through numerical integration of the following formulae for the ith component of displacement:

$$u_i(\boldsymbol{x}) = u_i^0(\boldsymbol{x}) + \int_L \phi_j(\boldsymbol{x}')G_{ij}(\boldsymbol{x}, \boldsymbol{x}')dL', \ i=1, 2, 3 \tag{24}$$

Equation (24) also needs to be discretized:

$$u_i(\boldsymbol{x}) = u_i^0(\boldsymbol{x}) + \sum_{m=1}^{M} \phi_j(\boldsymbol{x}_m')\overline{G}_{ij}(\boldsymbol{x}, \boldsymbol{x}_m'), \ i=1, 2, 3 \tag{25}$$

where the elements of $\{\overline{G}_{ij}\}$ are given in Appendices A and B.

In general, Eqs. (14-15) for SH-waves and (20-21) for P-SV waves form a system of 2M linear equations with 2M unknowns for the antiplane case (SH-wave), and 4M for the inplane case (P-SV-waves) for a general solid/solid interface, and can be further reduced if we consider some special cases, such as inclusionss filled with liquid or gas. For the non-viscous liquid case, the boundary conditions are the continuity of normal displacements and normal stress, and vanishing of shear stress. For the empty inclusion case, boundary conditions are the vanishing of both normal and shear stress (stress-free boundary conditions). In both cases S-wave displacement is

meaningless. For a detailed discussion, readers are directed to Coutant (1989) and Pointer, Liu and Hudson (1998).

The coefficient matrices of the equation systems (14-15) and (20-21) are fully populated complex matrices and are non-symmetric. This is often regarded as the disadvantage of BEM in comparison with finite element methods. Nevertheless, this matrix can be easily manipulated as the number of elements is not exceedingly high and the system of equations is only solved once for each frequency. A standard method such as the Gaussian elimination or *LU* decomposition method can be used, and for large M, a conjugate gradient method can be used. For examples presented in this paper, the number of boundary elements is not too large, therefore we only use a standard *LU* decomposition method to solve the linear equations. The maximum number of elements is restricted by the power of current computers and it also depends on the specified accuracy. In general, the number of elements depends on the particular frequency considered: at low frequencies, a minimum number of elements is required, while at high frequencies this number should be chosen such that at least three surface elements are sampled per seismic wavelength to give satisfactory results (Bouchon and Coutant, 1994).

IV. NUMERICAL EXAMPLES

Before we present numerical examples, it is necessary to mention that special care must be taken for corners and edges as the constant c_l given in Eq. (5) is not valid for non-smooth interfaces, such as corners or edges. There are two ways to circumvent this difficulty. The first and the simplest way is to take the field point to be slightly away from the corner by two separate nodes, i.e. by considering two corner nodes defined to be close to each other (typically 0.05 times the length of the local element apart). The second method is to re-calculate the constant c_l using its original definition for a given corner or edge. Banerjee and Butterfield (1981) also indicate that these two methods can give very similar results. In our implementation, we have used the first method. Note that the BEM formulations in the previous section are given for elastic inclusions, but for simplicity, we will only show examples for empty inclusions or cavities.

In the first test example, the inclusion was assigned the same material properties as the surrounding medium. Clearly, this test should produce the free-field conditions, and in fact it did. The program was subsequently validated by comparing our results with results obtained using similar approaches. Mal (1970) computed the crack opening displacement for various wavelengths of excitation using a boundary integral equation method which involves a P-wave normally incident on a very thin crack located in an infinite elastic medium. Our results are compared with his solution in Fig. 2. In our model the crack contour is represented by 80 points (40 points for each face of the crack), and each end of the crack is represented with an additional two points to make the crack tip smoother. The distance between the two faces of the cracks is given a finite value which may be chosen arbitrarily small. The particular value used here is 1/1000 the crack length. A good agreement has been achieved between our results and Mal's results (1970).

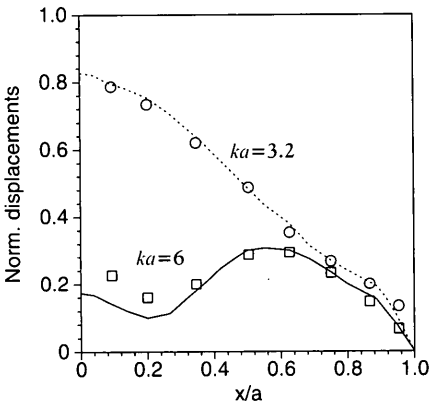

Fig. 2 Amplitude of the displacement of the face of a crack calculated using Mal (1970) for a vertically incident P-wave for two frequencies corresponding to ka=3.2 and ka=6. The result is normalised to the displacement at the centre of the crack. Curves are from Mal (1970) following Manolis and Besko (1988) and symbols are from the BEM studied in this paper

The first example is given in Fig. 3, which we attempt to model four different realisations of random distributions. In each model, there are 30 cavities (i.e. with stress-free boundary conditions) randomly distributed in a 120 m × 120 m area. Note that there is a problem of overlap of inclusion positions, and this was overcome automatically either by randomly moving adjacent inclusions so that the distance between the centre of adjacent inclusions is greater than the inclusion diameter, or by removing the overlapping inclusion and generating another inclusion until the desired number of inclusions is reached. The second method is used in all examples in this paper. As a result of this process, the final distribution is not necessarily completely random, nevertheless, the purpose of this paper is to illustrate the technique and to see how different distributions affect the multiple scattering. Each inclusion has a radius of a=2.5 m, and is discretized into 8 elements. The surrounding solid (matrix) has v_p=3500 m/s, v_s=2020 m/s, and density ρ= 2.3 gcm^{-3}. Plane wave sources are used. Plane waves travel along the

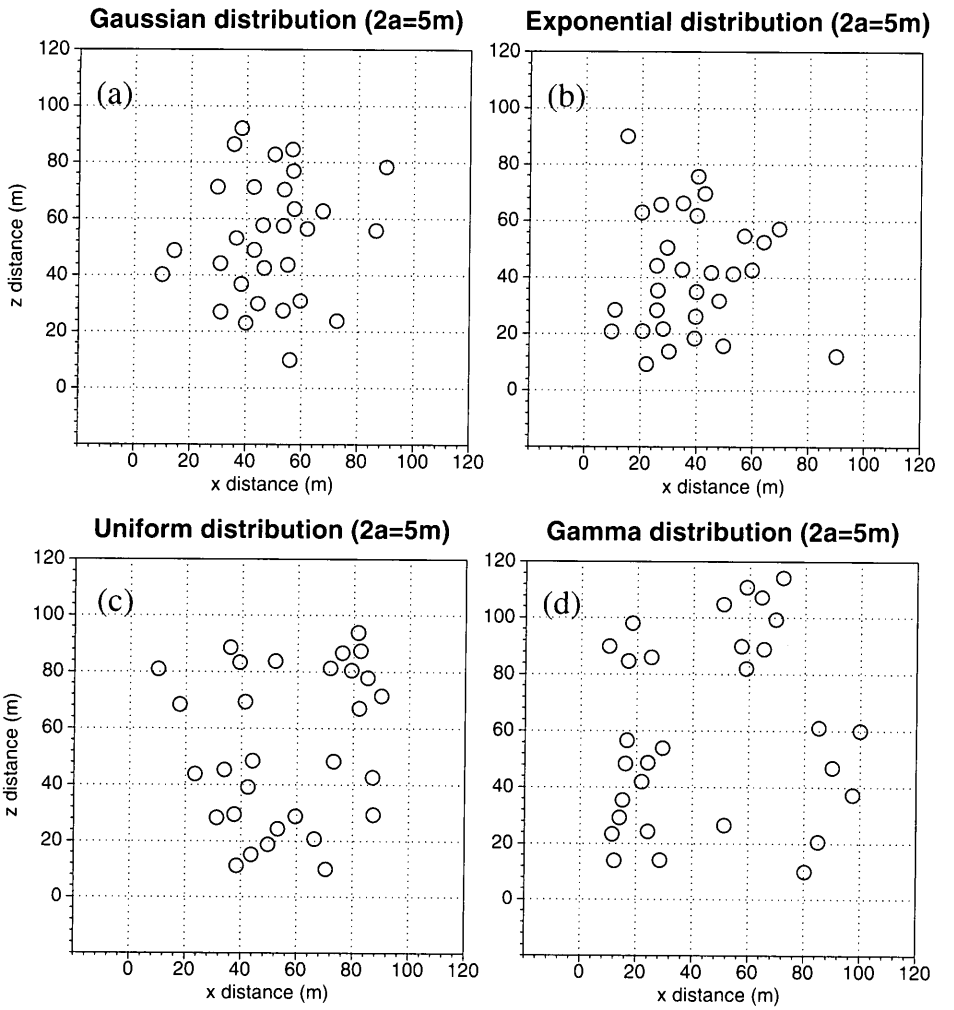

Fig. 3 Example 1: model used to compute synthetic seismograms from spatially distributed inclusions: (a) Gaussian, (b) exponential, (c) uniform; and (d) Gamma distributions. Plane waves (SH, SV and P) travel along the positive x-direction, and 90 receivers are located along the z-axis at x=120 m starting from z=150 m and with an increment of Δz=-1.6 m

positive x-direction, and 90 receivers are located along the z-axis at x=120 m starting from z=150 m and with an increment of Δz=-1.6 m. A Ricker wavelet with a dominant frequency of 100 Hz is used, so that $k_p a$=0.45, and $k_s a$=0.78 (k_p and k_s are P- and S-wavenumbers), or equivalently $\lambda_p/2a$=7 and $\lambda_s/2a$=4 (λ_p and λ_s are P- and S-wavelengths, respectively).

The resulting synthetic seismograms are given in Fig. 4 for SH-wave sources. The SH-waves are polarised out of plane in the y-direction, SV-waves in the z-direction and P-waves in the x-direction. The coda waves last shorter for the SH-waves from models (c) and (d) and this can be explained by the fact that inclusions are more clustered in the centre for models (a) and (b), whereas inclusions are more scattered or more uniformly distributed for models (c) and (d). This is exactly what we expected. A slight time delay can be seen in the middle of the plots (middle receivers) and this is due to the fact that the middle receivers are located immediately behind the inclusions so that more scattering interferences are expected.

Fig. 5 shows comparison of waveforms from the middle traces (number 45) of Fig. 4 and their corresponding Fourier spectra. It is apparent that the amplitudes from uniform and Gamma distributions (traces c and d) are much smaller and have relatively low frequency contents. The explanation is that for both of these two distributions, inclusions are distributed widely spread across the model areas, and scattered or coda waves last longer than from exponential and Gaussian distributions (a and b). Further analysis using the time-frequency analysis shown in Fig. 6 confirms not only the variation of frequency contents due to variation in position distributions, but also variation in duration of scattered or coda waves on the spatial variations. One of the advantages of the time-frequency analysis is that frequency contents from multiple arrivals, such as the scattered

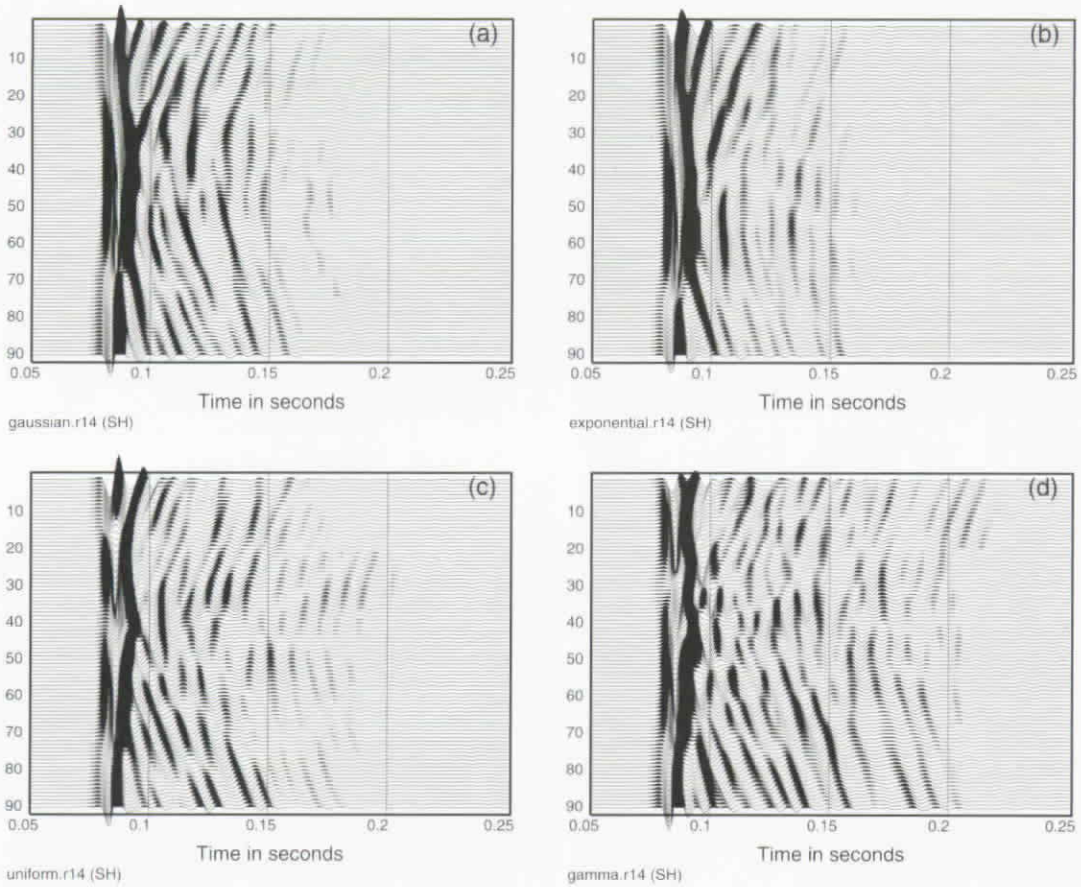

Fig. 4 Synthetic full wavefield from the plane SH-wave incidence. (a) to (d) correspond to distributions (a) to (d) in Figure 3. The numbers on the left side of the synthetic seismograms are the receiver numbers

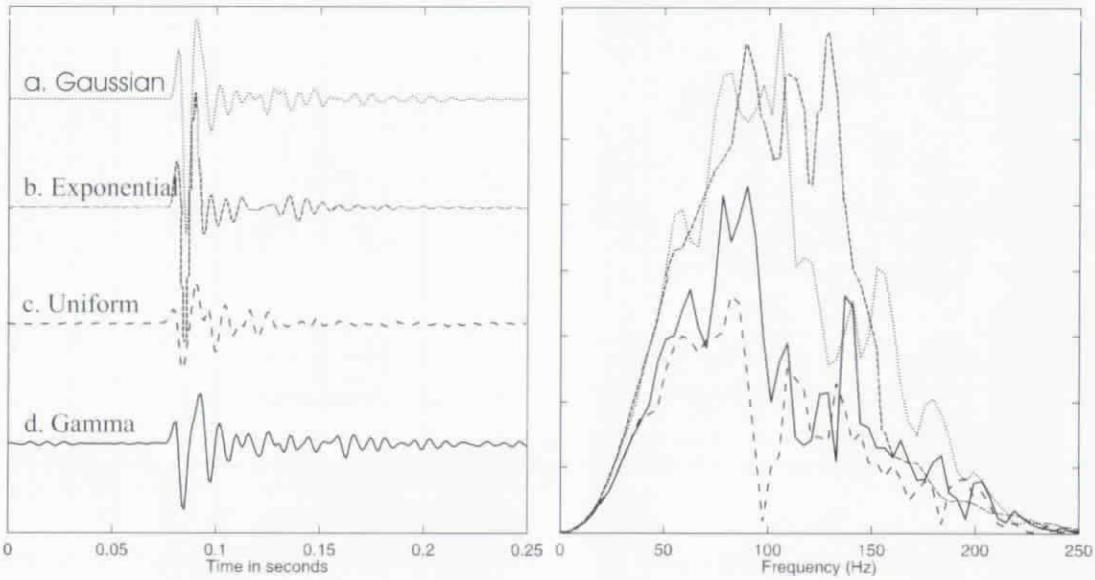

Fig. 5 Comparison of synthetic seismograms and corresponding spectra from various distributions in Figure 4 (trace number 45)

wavefields, can be identified. This example demonstrates that different distributions of inclusions have a significant influence on the multiple scattering.

Our second example is to demonstrate that BEM can be used to model wave scattering from discrete inclusions with scalelength distribution. The

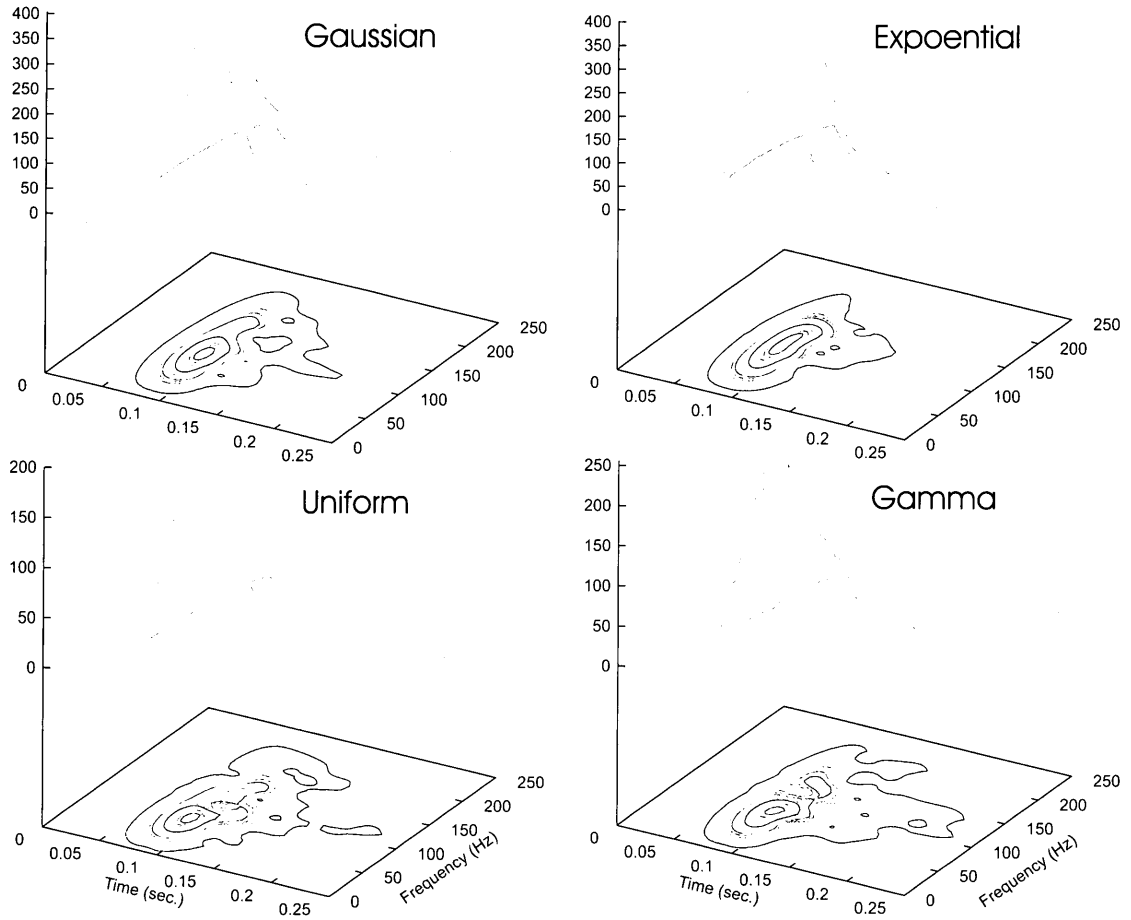

Fig. 6 Time-frequency analysis of synthetic traces in Figure 5

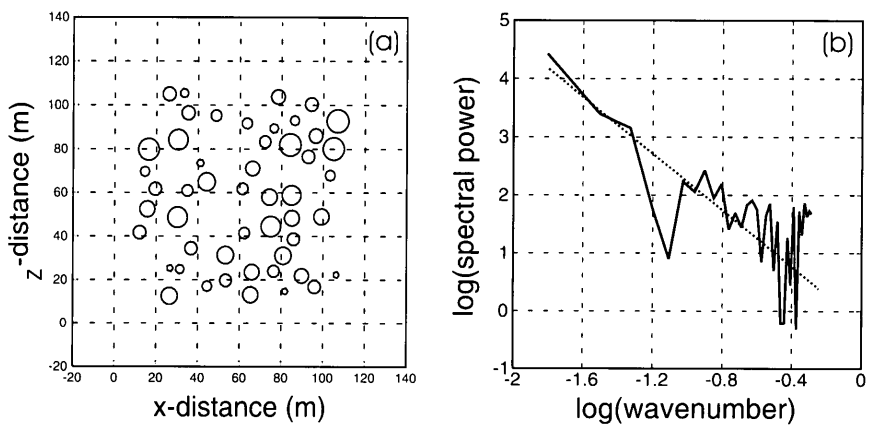

Fig. 7 Example 2: (a) model used to compute synthetic seismograms from inclusion distribution with power-law distribution of crack sizes. (b) Power spectra of size distributions as shown in (a) and Horizontal axis is spatial wavenumber (in log scale)

particular model that we use is given in Fig. 7a, where with variation of sizes follows a von Kármán correlation function. Other correlation functions, such as Gaussian or exponential functions can also be easily calculated, and the use of von Kármán correlation function is purely for mathematical convenience. Readers are referred to the paper by Ikelle, Yung and Daube (1993) for discussion about the generation of random media. The model given in Fig. 7a is generated with a correlation length of 3.5 m and variance of also equal to 3.5 m. The largest radius is 5.5 m and smallest is 1.25 m. The peak frequency is 100Hz, which gives ka ranging from 0.4 to 1.7 (k is wavenumber and shear-wave velocity is 2000 m/s).

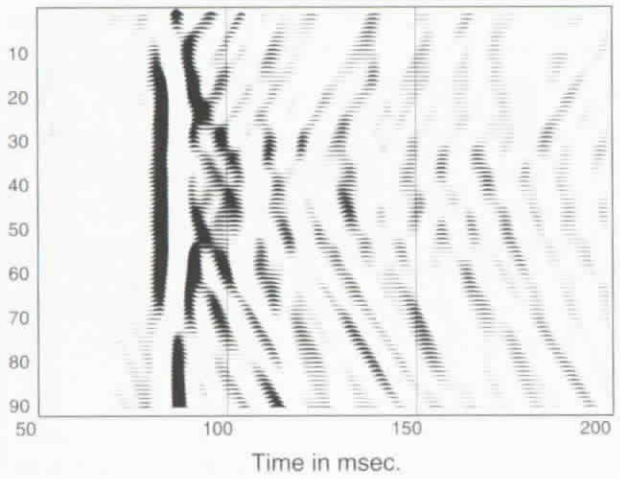

Fig. 8 Synthetic SH wavefield corresponding to model shown Figure 7a

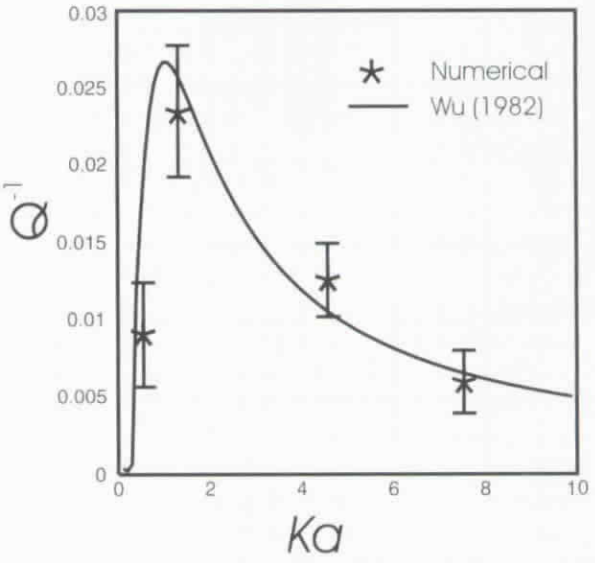

Fig. 9 Comparison of scattering attenuation estimated from synthetic seismograms shown in Figure 8 with by Wu's (1982) single scattering solution

The source and receiver positions are arranged in the same way as described in the earlier example (Figure 4). Fig. 7b shows the power spectrum of the size distributions shown in Fig. 7a (plotted in log-log scale), and as expected, the variation can be fitted with a straight line. Such a model, i.e. with linear variation of power spectrum with spatial wavenumber, is often called fractal or power-law distribution (Leary, 1997). The corresponding synthetic SH wavefield wavefield is given in Fig. 8. As we can see, the wavefield is quite complicated, and there is long duration of coda wave energy. Fig. 9 shows the comparison of scattering attenuation estimated from Fig. 8 with single scattering solution derived by Wu (1982). The scattered attenuation is estimated using the approach described by Yomogida, Aki and Benites (1997). We can see that there is a fairly good agreement between the BEM numerical results and single scattering solution of Wu (1982).

V. CONCLUSIONS

We have computed multiple scattering wavefields in media containing cracks or inclusions of various spatial distributions using the elastodynamic boundary element method. From this study, we can draw the following conclusions: (1) Scattering by cracks/inclusions can be solved relatively easily using the boundary element method. Multiple scattering can be included without additional difficulty. The method has unique advantages over other numerical methods in a number of ways. Its primary disadvantage lies in the difficulty of modelling lateral variation, and high computer costs when (and only when) there are many inclusions to be discretized. (2) Numerical studies show that in the presence of inclusions, spatial and scalelength distributions are important and cannot be ignored in modelling cracked rock. Different spatial arrangements of the same scatters lead to profound differences in scattering characteristics, in particular the frequency contents of the transmitted wavefields. The frequency characteristics, such as the frequency of the peak attenuation, can be related to spatial size parameters of the model. (3) The complex characteristics of scattering wavefields from our examples have two immediate implications: On the negative side, increases in complexity due to multiple inclusions generate incoherent background scattered wavefields that tend to complicate the observations. So the interpretation becomes more difficult; On the positive side, this provides more insight into the complex mechanism of multiple scattering. By careful analysis, it should in principle be possible to obtain more information about the nature of spatially distributed inclusions.

VI. ACKNOWLEDGEMENTS

We thank Tim Pointer, John Hudson, John Queen and David Booth for useful discussions. We also thank two anonymous reviewers and Prof.Alex Cheng for their constructive comments. Part of this work was done while the first author (EL) was a visiting scientist at Institute of Geophysics, Chinese Academy of Sciences in Beijing and the visit was supported by the K.C. Wang Science Foundation (Hong Kong) in 1998. This paper is published with the approval of the Director of the British Geological Survey (NERC).

REFERENCES

1. Banerjee, P.K., and Butterfield, R., 1981, *Boundary element methods in engineering science*, McGraw-Hill, London.
2. Bouchon, M., 1987, "Diffraction of Elastic Waves by Cracks or Cavities Using the Discrete Wavenumber Method," *Journal of Acoustical Society of America*, Vol. 81, pp.1671-1676.
3. Bouchon, M., and Coutant, O., 1994, "Calculation of Synthetic Seismograms in a Lateral Varying Medium by the Boundary Element-discrete Wavenumber Method," *Bulletin of Seismological Society of America*, Vol. 84, pp.1869-1881.
4. Chen, G., and Zhou, H.W, 1994, "Boundary element modelling of nondissipative and dissipative waves," *Geophysics*, Vol. 59, pp. 113-118.
5. Coutant, O., 1989, "Numerical Study of the Diffraction of Elastic Waves by Fluid-filled Cracks," *Journal of Geophysical Research-Solid Earth*, Vol. 94, pp. 17805-17818.
6. Cruse, T.A., 1968, "A Direct Formulation and Numerical Solution of the General Transient Elastodynamic Problem," *Journal of Mathematical Analysis Application*, Vol. 22, pp. 341-355.
7. Dong, W., and Toksöz, M.N., 1995, "Borehole Seismic-source Radiation in Layered Isotropic and Anisotropic Media: Boundary Element Modelling," *Geophysics*, Vol. 60, pp. 748-757.
8. Fehler, M., and Aki, K., 1978, "Numerical Study of Diffraction of Plane Elastic Waves by a Finite Crack with Application to Location of a Magma Lens", *Bulletin of Seismological Society of America*, Vol. 68, pp. 573-598.
9. Hudson, J.A., 1977, "Scattered Wave in the Coda of P," *Journal of Geophysics*, Vol. 43, pp. 359-374.
10. Hudson, J.A., 1981, "Wave Speeds and Attenuation of Elastic Waves in Material Containing Cracks," *Geophysical Journal of Royal Astronomical Society*, Vol. 64, pp.133-150.
11. Hudson, J.A., and Heritage, J.R., 1981, "The Use of the Born Approximation in Seismic Scattering Problems," *Geophysical Journal of Royal Astronomical Society*, Vol. 66, pp. 221-240.
12. Ikelle, K.T., Yung, S.K., and Daube, F., 1993, "2D Random Media with Ellipsoid Correlation Function," *Geophysics*, Vol. 58, pp. 1359-1372.
13. Liu, E., Crampin, S., and Hudson, J.A., 1997, "Diffraction of Seismic Waves by Cracks with Application to Hydraulic Fracturing," *Geophysics*, Vol. 62, pp. 253-265.
14. Mal, A.K., 1970, "Interaction of Elastic Waves with a Penny-shaped Crack," *International Journal of Engineering Science*, Vol. 8, pp. 381-388.
15. Manolis, G.D., and Besko, D.E., 1988, *Boundary Element Methods in Elastodynamics*, Unwin Hyman, London.
16. Murai, Y., Kawahara, J., and Yamashita, T., 1995, "Multiple Scattering of SH-waves in 2D Elastic Media with Distributed Cracks," *Geophysical Journal International*, Vol. 122, pp. 925-937.
17. Pao, Y.H., and Varatharajulu, V., 1976, "Huygens' Principle, Radiation Conditions, and Integral Formulas for the Scattering of Elastic Waves," *Journal of Acoustical Society of America*, Vol. 59, pp. 1361-1371.
18. Pointer, T., Liu, E., and Hudson, J.A., 1998, "Numerical Modelling of Seismic Waves Scattered by Hydrofractures: Application of the Indirect Boundary Element Method," *Geophysical Journal International*, Vol. 135, pp.289-303.
19. Sánchez-Sesma, F.J., and Campillo, M., 1991, "Diffraction of P, SV, and Rayleigh Waves by Topographic Features: a Boundary Integral Formulation," *Bulletin of Seismological Society of America*, Vol. 81, pp. 2234-2253.
20. Sánchez-Sesma, F.J., and Campillo, M., 1993, "Topographic Effects for Incident P, SV, and Rayleigh Waves," *Tectonophysics*, Vol. 218, pp. 113-125.
21. Wu, R.-S., 1982, "Attenuation of Short Period Seismic Waves Due to Scattering," *Geophysical research Letter*, Vol. 9, pp. 9-12.
22. Yokoi, T., 1996, "Numerical Study on the Generation of Downgoing S-waves by a Vertical Force Acting Close to a Step-like Topography," *Geophysics*, Vol. 61, pp.192-201.
23. Yomogida, K., Aki, K., and Benites, R.,1997, "Coda Q in Two-layer Random Media," *Geophysical Journal International*, Vol. 128, pp. 425-433.

APPENDIX

A. Coefficients for SH-waves

The coefficient matrix elements in equations (14-15) are given by:

$$A_{nm} = \overline{G}_{22}(\boldsymbol{x}_n, \boldsymbol{x}_m) = \int_{\Delta L_m} G_{22}(\boldsymbol{x}_n, \boldsymbol{x}_m) dL' , \qquad \text{(A1)}$$

$$B_{nm} = -\frac{1}{2}\delta_{nm} + \overline{T}_{22}(\boldsymbol{x}_n, \boldsymbol{x}_m) = -\frac{1}{2}\delta_{nm} + \int_{\Delta L_m} T_{22}(\boldsymbol{x}_n, \boldsymbol{x}_m) dL' , \qquad \text{(A2)}$$

$$A'_{nm} = -\overline{G}'_{22}(\boldsymbol{x}_n, \boldsymbol{x}_m) = -\int_{\Delta L_m} G'_{22}(\boldsymbol{x}_n, \boldsymbol{x}_m) dL' , \qquad \text{(A3)}$$

and

$$B'_{nm} = -\frac{1}{2}\delta_{nm} - \overline{T}'_{22}(\boldsymbol{x}_n, \boldsymbol{x}_m)$$

$$= -\frac{1}{2}\delta_{nm} - \int_{\Delta L_m} T'_{22}(\boldsymbol{x}_n, \boldsymbol{x}_m)dL' . \quad \text{(A4)}$$

Equation (A2) and (A4) become

$$B_{nm} = B'_{nm} = -\frac{1}{2}, \text{ if } n=m, \quad \text{(A5)}$$

when $\boldsymbol{x}_n$ approaches $\boldsymbol{x}_m$ (Banerjee and Butterfield, 1984; Pointer *et al.*, 1998). In all cases, n, m=1, 2, ..., M.

B. Coefficients for P-SV-waves

The coefficient matrix elements in Eqs. (20-21) are given by:

$$A^{ij}_{nm} = \overline{G}_{ij}(\boldsymbol{x}_n, \boldsymbol{x}_m) = \int_{\Delta L_m} G_{ij}(\boldsymbol{x}_n, \boldsymbol{x}_m)dL' , \quad \text{(B1)}$$

$$B^{ij}_{nm} = -\frac{1}{2}\delta_{nm}\delta_{ij} + \overline{T}_{ij}(\boldsymbol{x}_n, \boldsymbol{x}_m)$$

$$= -\frac{1}{2}\delta_{nm}\delta_{ij} + \int_{\Delta L_m} T_{ij}(\boldsymbol{x}_n, \boldsymbol{x}_m)dL' , \quad \text{(B2)}$$

$$A^{ij}_{nm} = -\overline{G}'_{ij}(\boldsymbol{x}_n, \boldsymbol{x}_m) = -\int_{\Delta L_m} G'_{ij}(\boldsymbol{x}_n, \boldsymbol{x}_m)dL' , \quad \text{(B3)}$$

and

$$B'^{ij}_{nm} = -\frac{1}{2}\delta_{nm}\delta_{ij} - \overline{T}'_{ij}(\boldsymbol{x}_n, \boldsymbol{x}_m)$$

$$= -\frac{1}{2}\delta_{nm}\delta_{ij} - \int_{\Delta L_m} T'_{ij}(\boldsymbol{x}_n, \boldsymbol{x}_m)dL' . \quad \text{(B4)}$$

Equation (B2) and (B4) become

$$B^{ij}_{nm} = B'^{ij}_{nm} = -\frac{1}{2}\delta_{ij}, \text{ if } n=m, \quad \text{(B5)}$$

when $\boldsymbol{x}_n$ approaches $\boldsymbol{x}_m$ (Banerjee and Butterfield, 1984; Pointer *et al.*, 1998). In all cases, i, j= 1, 3, and n, m=1, 2, ..., M.

Discussions of this paper may appear in the discussion section of a future issue. All discussions should be submitted to the Editor-in-Chief.

Manuscript Received: Nov. 18, 1999
Revision Received: Feb. 20, 2000
and Accepted: Feb. 28, 2000

空間分佈置入物的彈動力多重散射問題

Enru Liu 與 Zhongjie Zhang

British Geological Survey, Murchison House, West Mains Road
Edinburgh EH9 3LA, Scotland UK
Institute of Geophysics, Chinese Academy of Sciences
11 Datun Road, Beijing, China 100101

摘 要

本文採用二維彈動力積分方程或邊界元素法來解裂縫散射的問題。本法是以散射波場的積分表示式爲基礎，假設一個虛擬源分佈在散射物體或置入物上（亦即數學上所描述的惠更斯原理），而且這個虛擬源的分佈強度可以在置入物的邊界配合適當的邊界條件來決定。我們舉出兩個數值的算例來說明邊界元素法的可行性。第一個算例顯示出對相同的散射體而言，不同空間的安排將導致非常不同的散射特性，特別是在經由時頻分析後之透射波之頻率內涵。第二個算例說明了透射波場受乘冪律與尺寸效應之碎形分布的影響，波峰衰減的頻率特性是與模式中之空間尺寸參數有關的。

關鍵字：彈動力邊界元素法，置入物，彈性波，多重散射。